Fusion Engineering and Design 216 (2025) 115049

Contents lists available at ScienceDirect

Fusion Engineering and Design

journal homepage: www.elsevier.com/locate/fusengdes

Energy optimization of the EFCC power supply in DTT scenarios

Pasquale Zumbolo [a,b,*], Raffaele Albanese [a,b,c], Andrea G. Chiariello [a,d], Antonio Iaiunese [a,e], Alessandro Lampasi [c,f], Marco Neri [a,b,g], Raffaele Martone [a,c]

[a] Consorzio CREATE, Via Claudio 21, Naples, 80125, Italy
[b] Università degli Studi di Napoli Federico II, Via Claudio 21, Naples, 80125, Italy
[c] DTT S.C. a r.l., Via E. Fermi 45, Frascati, 00044 Rome, Italy
[d] Università degli Studi della Campania "L. Vanvitelli", Via Roma 29, Aversa (Caserta) 81031, Italy
[e] Università degli Studi di Napoli Parthenope, Centro Direzionale Isola C4, Naples, 80143, Italy
[f] ENEA, Nuclear Department, Via E. Fermi 45, Frascati, 00044 Rome, Italy
[g] Università degli Studi di Padova, Corso Stati Uniti 4, Padua, 35127, Italy

ARTICLE INFO

Keywords:
Tokamak
Error fields
Power supply
Energy consumption

ABSTRACT

The Divertor Tokamak Test facility comprises a sophisticated system designed to counteract Error Fields. The actual field correction demand will depend on the final characteristics of the assembled machine and, during operations, on the specific scenario instant. In this work, a comprehensive approach for the optimal design of the Error Field Correction Coil currents during the scenario is presented; the model is based on a circuit model of magnetic sources, including the correction coils, as well as Poloidal Field coils, Central Solenoid, plasma current and eddy currents. The available degrees of freedom are exploited to minimize the energy demand from correction coils power supplies while ensuring effective reduction of Error Fields.

1. Introduction

Error Field Correction Coils (EFCCs) are non-axisymmetric coils included in a tokamak design to counteract Error Fields (EFs) due to nonidealities in the desired magnetic configuration. Their function is crucial to maintain plasma stability and avoid the formation of locked modes and, ultimately, disruptions [1–5].

The design of the EFCCs is a significant challenge since the actual EFs to be counteracted are unknown until the machine is fully assembled. Furthermore, the EFs depend on the specific operating conditions and, in addition, on the possible safety margins that might be introduced instant by instant for prudential reasons. Therefore, a dynamic EF correction action should be investigated. In addition, the EFCC demand in terms of electric energy and EF correction conflicts with other requirements, such as edge localized modes mitigation and, as future deployment, neoclassical toroidal viscosity control [6].

In the recent past, the EFCC currents have been calculated considering the EF correction for just a single scenario instant [7–10].

However, the actual EFs to be counteracted depend on the plasma equilibria of the considered scenario and change during a pulse, according to the evolution of the currents in the magnetic field sources, namely Poloidal Field (PF) coils and Central Solenoid (CS), eddy currents and plasma shape and current. Therefore, a flexible tool to aid in choosing the EFCCs currents throughout the scenario, exploiting the degrees of freedom to optimize the energy consumption, has been developed.

The procedure described in this work is based on a comprehensive model able to treat the complex interactions between the EFCCs power supplies and the other sources during a complete scenario, considering the electrical characteristics of the coils, the inductive couplings and both the time-varying shape and position of the plasma.

The objective is to optimize the EFCC currents to minimize both energy consumption and the impact of EFs, while ensuring various constraints.

The plasma reaction may significantly affect the EFs distribution; following the present available studies, the expected impact can be either an amplification or a shielding [6,11–13]; here, for simplicity reasons, to estimate the impact of the EFs as a function of correction currents, the standard vacuum response metric "Three Mode Error Index" (*TMEI*) is used [7,8].

The optimization problem is formulated using a quadratic programming approach [14,15], taking into account the non-linearity of the

* Corresponding author at: Consorzio CREATE, Naples, Italy.
E-mail address: pasquale.zumbolo@unina.it (P. Zumbolo).

https://doi.org/10.1016/j.fusengdes.2025.115049
Received 27 November 2024; Received in revised form 21 March 2025; Accepted 2 April 2025
Available online 16 April 2025

objective function and the presence of multiple constraints, such as voltage and current limits. The result is the optimal sequence of EFCC currents for the given scenario, able to guarantee efficient and effective control of EFs.

Although this study is part of a package of EF analysis for the Divertor Tokamak Test (DTT) EFCC system, the mathematical formulation and the optimization procedure have been developed as general tools for the design and operation of the EF correction system in any tokamak device.

The paper is organized as follows: Section 2 covers the mathematical model, with circuit equations, assumptions, matrix formulation, and energy optimization problem. Section 3 discusses the results, and Section 4 presents the conclusions.

2. Mathematical model

2.1. Circuit model: matrix formulation

For the purposes of this work, the EFCC currents have been assumed as unknowns in the mathematical model, while they are assumed to be known in all the other coupled circuits, along the whole scenario.

The voltages of the EFCCs are calculated both to assess the electric power requirements and to enforce physical constraints. while those on the other circuits are not required as they are assumed to be current-driven.

Furthermore, the effects of ferromagnetic materials are neglected, and no time-dependance of the inductances coefficients between the coils is taken into account ("*shape invariance*" assumption). The resulting model is linear.

The voltage at the j-th ($j = 1, \ldots, K_{cc}$) EFCC, with a standard convention, is given by:

$$v_j(t) = v_j^{cc}(t) + R_j i_j^{cc}(t) + v_j^{eq}(t) + +v_j^{pl}(t) + v_j^{eddy}(t) \tag{1.1}$$

where K_{cc} is the number of EFCCs, $v_j^{cc}(t)$ is the inductive contribution of the overall EFCC system, R_j is the resistance of the j-th EFCC, $v_j^{eq}(t)$ the contribution due to the PF/CS, $v_j^{pl}(t)$ the contribution due to the plasma, and, finally, $v_j^{eddy}(t)$ is the eddy current contribution due to the surrounding conductive structures.

The contribution $v_j^{cc}(t)$ has the following expression:

$$v_j^{cc}(t) = \sum_{k=1}^{K_{cc}} M_{j,k}^{cc} \frac{di_k^{cc}(t)}{dt} \tag{1.2}$$

where $M_{j,k}^{cc}$ is the mutual inductance with the k-th EFCC. Similarly, it results:

$$v_j^{eq}(t) = \sum_{k=1}^{K_{eq}} M_{j,k}^{eq} \frac{di_k^{eq}(t)}{dt} \tag{1.3}$$

where $M_{j,k}^{eq}$ is the mutual inductance with the k-th PF/CS and K_{eq} is the total number of PF and CS circuits.

The term due to plasma, $v_j^{pl}(t)$ is:

$$v_j^{pl}(t) = \frac{d\left(M_j^{pl} i^{pl}\right)}{dt} \tag{1.4}$$

where a time evolution of the mutual inductance with the plasma current is also considered to take into account its geometrical variations as well as the evolution of the current profile. Note that v_j^{eq}, v_j^{pl} and v_j^{eddy} are known terms of the model.

Eq. (1.1) can be rewritten in vector form:

$$\underline{v}(t) = \underline{\underline{M}}^{cc} \frac{d\underline{i}^{cc}}{dt} + \underline{\underline{R}}^{cc} \underline{i}^{cc}(t) + \underline{v}^{eq}(t) + \underline{v}^{pl}(t) + \underline{v}^{eddy}(t) \tag{2}$$

where $\underline{v}(t)$ collects, at j-th position (with $j = 1, \ldots, K_{cc}$), the voltage at the j-th EFCC at instant t; similar meanings have the arrays $\underline{v}^{eq}, \underline{v}^{pl}$ and $\underline{v}^{eddy}$ for the other voltages and $\frac{d\underline{i}^{cc}}{dt}$ and $\underline{i}^{cc}$ for the currents; in addition, is the inductance matrix of the EFCC system and $\underline{\underline{R}}^{cc}$ its diagonal matrix of resistances.

The energy absorbed by the EFCC circuits until the generic instant τ is:

$$w(\tau) = \int_{-\infty}^{\tau} \underline{v}(t)^T \underline{i}^{cc}(t)\, dt \tag{3}$$

By minimizing a cost function containing (3), the K_{cc} EFCC current waveforms in the array $\underline{i}^{cc}(t)$ are evaluated, throughout the scenario, so as to both counteract the EFs and minimize the energy demand, within the current and voltage constraints of the power supply.

2.2. Finite-dimensional model: $\underline{i}^{cc}$ linear time behavior

To simplify the mathematical treatment, the current waveforms are projected in the linear piecewise function space. More complex approximations might be envisaged but the linear approximation accuracy can be satisfactory if the time ranges are sufficiently small. In the generic time interval $\Delta t_n = t_n - t_{n-1}$, within the scenario timeframe $[t_0, t_N]$ (with $n = 1, \cdots, N$ and N the number of intervals), the EFCC currents can be expressed as:

$$\underline{i}_n^{cc}(t) = \underline{i}_n^{cc}(t_{n-1}) + \frac{\Delta \underline{i}_n^{cc}}{\Delta t_n}\ (t - t_{n-1}) \tag{4}$$

where $\Delta \underline{I}_n^{cc}$ is the array of the EFCC current variations at the interval extreme values and $\underline{i}_n^{cc}(t_{n-1})$ collects the K_{cc} currents at t_{n-1} instant of the interval $[t_{n-1}, t_n]$. Note that the EFCC currents are state variables; therefore, the continuity between the consecutive intervals sharing the instant t_n must be imposed, namely $\underline{i}_n^{cc}(t_n) = \underline{i}_{n+1}^{cc}(t_n)$.

Similar expressions can be written also for PF/CS currents, eddy currents and for plasma current.

A piecewise linear time behaviour for plasma mutual inductance has been assumed as well. Therefore, from (1.4) the plasma voltage contributions can be expressed as:

$$\underline{v}_n^{pl}(t_{n-1}) = \underline{M}^{pl}(t_{n-1}) \frac{\Delta i_n^{pl}}{\Delta t_n} + i^{pl}(t_{n-1}) \frac{\Delta \underline{M}_n^{pl}}{\Delta t_n} \tag{5}$$

where the array $\Delta \underline{M}_n^{pl}$ collects the K_{cc} variations of the mutual coupling between EFCCs and plasma current at the extremes of the interval and Δi_n^{pl} is the plasma current variation.

As a consequence, the voltages of the EFCCs are linear piecewise waveforms in Δt_n:

$$\underline{v}_n(t) = \underline{v}_n(t_{n-1}) + \frac{\Delta \underline{v}_n}{\Delta t_n}\ (t - t_{n-1}) \tag{6.1}$$

where:

$$\Delta \underline{v}_n = \underline{\underline{R}}^{cc} \Delta \underline{i}_n^{cc} + \Delta \underline{v}_n^{pl} \tag{6.2}$$

and:

$$\begin{aligned} \underline{v}_n(t_{n-1}) = {} & \underline{\underline{M}}^{cc} \frac{\Delta \underline{i}_n^{cc}}{\Delta t_n} + \underline{\underline{R}}^{cc} \underline{i}^{cc}(t_{n-1}) + \ldots \\ & + \underline{v}_n^{pl}(t_{n-1}) + \underline{v}_n^{eq}(t_{n-1}) + \underline{v}_n^{eddy}(t_{n-1}) \end{aligned} \tag{6.3}$$

2.3. Energy evaluation

From (3) it is possible to show that the amount of energy required by the EFCC system in Δt_n is:

$$w_n = \underline{x}^T \underline{\underline{A}}^{(n)} \underline{x} + \underline{x}^T \underline{b}^{(n)} \tag{7.1}$$

with $\underline{x} = \begin{bmatrix} \underline{x}_{n-1} \\ \underline{x}_n \end{bmatrix} = \begin{bmatrix} \underline{i}_n^{cc}(t_{n-1}) \\ \underline{i}_n^{cc}(t_n) \end{bmatrix}$ where the block matrix $\underline{\underline{A}}^{(n)}$ is:

$$\underline{\underline{A}}^{(n)} = \left[\begin{array}{c|c} -\frac{1}{2}\underline{\underline{M}}^{cc} + \frac{\Delta t_n}{3}\underline{\underline{R}}^{cc} & \frac{\Delta t_n}{6}\underline{\underline{R}}^{cc} \\ \hline \frac{\Delta t_n}{6}\underline{\underline{R}}^{cc} & \frac{1}{2}\underline{\underline{M}}^{cc} + \frac{\Delta t_n}{3}\underline{\underline{R}}^{cc} \end{array}\right] \tag{7.2}$$

and the array$\underline{b}^{(n)}$ is:

$$\underline{b}^{(n)} = \begin{bmatrix} \frac{\Delta \underline{v}_n^{pl}}{6} + \frac{\left(\underline{v}_n^{pl}(t_{n-1}) + \underline{v}_n^{eq}(t_{n-1}) + \underline{v}_n^{eddy}(t_{n-1})\right)}{2} \\ \frac{\Delta \underline{v}_n^{pl}}{3} + \frac{\left(\underline{v}_n^{pl}(t_{n-1}) + \underline{v}_n^{eq}(t_{n-1}) + \underline{v}_n^{eddy}(t_{n-1})\right)}{2} \end{bmatrix} \Delta t_n \tag{7.3}$$

In the subsequent step-by-step optimization procedure, N optimization steps have to be carried out sequentially on all the sequence of N intervals. At each step the $\underline{x}_{n-1}$ is assigned (starting from $\underline{x}_0$) because of the current continuity; therefore (7.1) can be rewritten in a simpler form:

$$w_n = \underline{x}_n^T \underline{\underline{A}}_{22}^{(n)} \underline{x}_n + \underline{x}_n^T \left[\underline{b}_2^{(n)} + 2\underline{\underline{A}}_{21}^{(n)} \underline{x}_{n-1}\right] + k_{n-1} \tag{8.1}$$

where:

$$k_{n-1} = \underline{x}_{n-1}^T \underline{\underline{A}}_{11}^{(n)} \underline{x}_{n-1} + \underline{x}_{n-1}^T \underline{b}_1^{(n)} \tag{8.2}$$

and $\underline{\underline{A}}_{11}^{(n)}$, $\underline{\underline{A}}_{21}^{(n)}$ and $\underline{\underline{A}}_{22}^{(n)}$ are the submatrices which notation follows the common partitioning of $\underline{\underline{A}}^{(n)}$, as well as $\underline{b}_1^{(n)}$ and $\underline{b}_2^{(n)}$ the partitioning for $\underline{b}^{(n)}$.

2.4. Energy and EF optimization

The aim of the EFCC system is to counteract EFs along the scenario.

As mentioned in the introduction, the *TMEI* metric for the EF estimation has been adopted in this work. The *TMEI* at a generic instant t_n of a scenario can be expressed as:

$$TMEI_n = \frac{\sqrt{\underline{x}_n^T \underline{\underline{G}}^{(n)^T} \underline{\underline{W}} \underline{\underline{G}}^{(n)} \underline{x}_n - 2\underline{x}_n^T \underline{\underline{G}}^{(n)^T} \underline{\underline{W}} \underline{f}_n + \underline{f}_n^T \underline{\underline{W}} \underline{f}_n}}{B_t} \tag{9}$$

where $\underline{f}_n$ collects the real and imaginary parts of the first three Fourier harmonics of the EF at t_n, $\underline{\underline{G}}^{(n)}$ is a matrix which collects the real and imaginary parts of the harmonics generated by unitary EFCC currents, $\underline{\underline{W}}$ is the diagonal matrix of the *TMEI* harmonics weights and B_t the unperturbed toroidal field at the magnetic axis [7,8].

In the design approach used in the past, the currents were evaluated instant by instant taking into account only the *TMEI*, and just the constraint on maximum current were imposed [8].

The procedure proposed here select the currents with the additional goal of reducing the energy required by the EFCC power supply. Then, the new formulation looks for the minimization of a new cost function containing both $TMEI_n$ and energy, together with two constraints, i.e., current and voltage.

The solution might be sought in different ways, such as minimizing

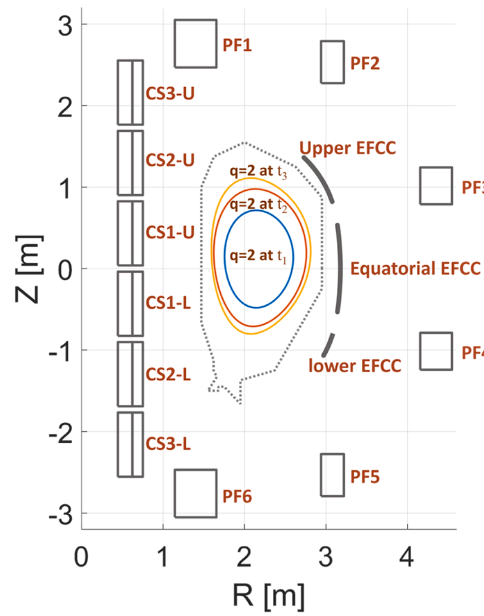

Fig. 1. DTT poloidal section including PF coils, CS coils, EFCCs and plasma q=2 surfaces at t_1, t_2 and t_3.

(8.1) and imposing the maximum allowed value of $TMEI_n$ as just a nonlinear inequality constraint or, alternatively, using one of the several multi-objective approaches.

Here, a multi-objective optimization approach based on the “penalty technique” is preferred due to its wide and effective flexibility. Then, (8.1) and (9) are combined providing, for the interval Δt_n, a scalar function well suited to be minimized, according to the classical single-objective optimization techniques:

$$\min_{\underline{x}_n}\{\alpha\, \lambda_1 w_n + (1-\alpha)\lambda_2 < TMEI_n > \} \tag{10}$$

where $< TMEI_n >$ is the interval average *TMEI* computed as $< TMEI_n > = (TMEI_n + TMEI_{n-1})/2$, λ_1 and λ_2 are suitable normalization factors used for scaling the two physical quantities to the same scale (actually the unity), and $\alpha \in [0,1]$ is the tunable weighting coefficient. In particular, the case $\alpha=0$ coincides with the old optimization procedure [8], while $\alpha=1$ provides the case of absence of EF correction effort. It is interesting to note that minimizing (10) for each value of the parameter α in [0,1], a set of optimal solutions is identified (“Pareto front” in the multi objectives optimization language), each associated with a specific value of α [16,17].

3. Results

The procedure has been applied to the DTT EFCC system to assess its effectiveness. DTT is equipped with 27 EFCC independent circuits, subdivided into three poloidal arrays (9 uppers, 9 equatorials and 9 lowers). The magnetic system (PF and CS coils) as well as the three EFCC arrays and plasma q=2 poloidal sections at different scenario instants are reported in Fig. 1. It is worth noticing that the term $v_j^{eddy}(t)$ can be neglected in DTT because the toroidal $n=0$ time constant of the vessel is about tens of milliseconds and even faster for $n>0$, while the time variation of the equilibrium currents is on the order of seconds [18].

The scenario considered here refers to a relevant divertor configuration [19]. The EFs, depending on manufacturing and assembly inaccuracies of the actual magnetic system, are currently unknown because DTT is still in the construction phase. However, the case studied here has been chosen from the worst-cases class, falling into 95 % of instances generated from a statistical analysis carried out in the past [20]. The maximum *TMEI* assumed for DTT is $TMEI_{limit}$=50 ppm.

Table 1
EFs optimization: TMEI reduction.

Instant	t_1=7.5 s	t_2=11 s	t_3=13.75 s
Plasma current	3 MA	4.4 MA	5.5 MA
$TMEI_{\mathrm{initial}}$	100 ppm	114 ppm	128 ppm
$TMEI_{\mathrm{corrected}}$	1 ppm	6 ppm	27 ppm
w	//	8.37 MJ	4.03 MJ

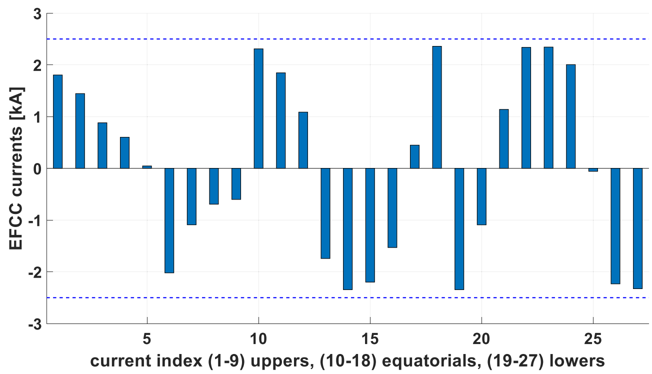

Fig. 2. EFCCs' optimized currents at t_1 with α=0 and current bounds (dashed horizontal lines).

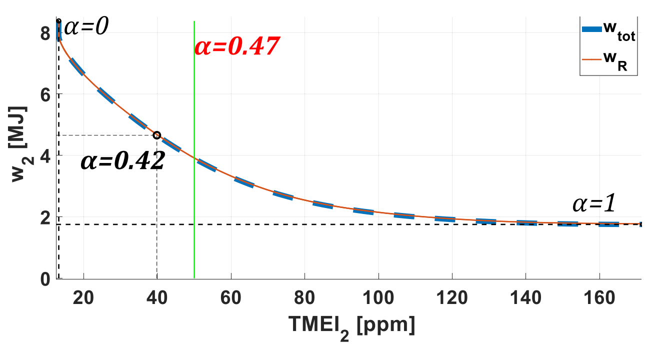

Fig. 3. EFCC energy demand in [t_1, t_2] versus $TMEI_2$ as solution of (10) varying α in [0,1] (blue dashed Pareto front), and its ohmic contribution versus $TMEI_2$ (red Pareto front).

To test the methodology performance, just a set of three consecutive instants (t_1=7.5 s, t_2=11 s, t_3=13.75 s) has been chosen within the scenario. The three instants were selected to examine both large and small variations in the q=2 surfaces, in order to emphasize the role of the plasma voltage contributions in (5). Furthermore, the following current and voltage constraints have been considered together with (2) according to the power supply specifications:

$$\left|v_j(t)\right| < 400 \text{ V} \tag{11.1}$$

$$\left|i_j^{cc}(t)\right| < 2.5 \text{ kA} \tag{11.2}$$

with $j = 1, \ldots, K_{cc}$.

3.1. Single objective-optimization: EF reduction

The EFs correction action, addressed as the optimization problem (10) in the α=0 case, was performed independently at the three time instants. A different iterative solver 'fmincon', available in MATLAB®, has been here preferred over 'quadprog', which was used in the past because of its larger flexibility in handling multi-objective function optimization problems [14,15]. Table 1 reports the three independent EF correction, together with the resulting energy consumption in the two intervals [t_1, t_2] and [t_2, t_3], calculated from (8.1) considering EFCC currents obtained from (10) with α=0.

Fig. 2 reports the EFCC currents at instant t_1. Note that several currents approach to the preset limits, this might reduce the redundance of the correction system and, as a consequence, its robustness versus possible coil/power supply failures.

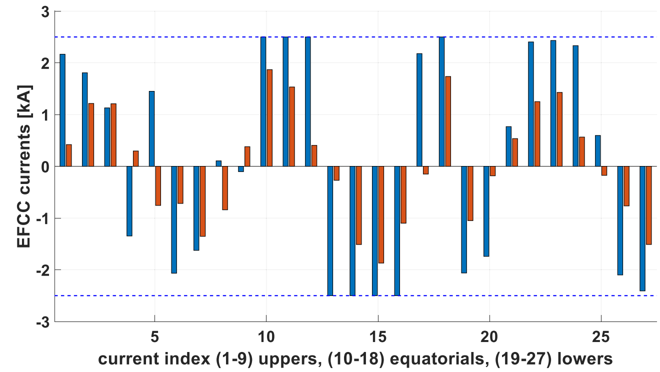

Fig. 4. EFCCs' optimized currents at t_2 instant: with α=0.42 (red bars), α=0 (blue bars) and current bounds (dashed horizontal lines).

Table 2
Energy contributions in [t_1, t_2] at main α values.

	w_R	w_L	w_{eq}	w_{pl}
α=0	8.37 MJ	13.5 kJ	-6.27 kJ	-0.86 kJ
α=0.42	4.67 MJ	-1.72 kJ	-1.78 kJ	-1.44 kJ
α=1	1.77 MJ	-22.0 kJ	-0.99 kJ	0.14 kJ

3.2. Multi-objective optimization: EF and energy reduction

The results in Section 3.1, i.e., $TMEI_{\mathrm{corrected}}$ much lower than $TMEI_{\mathrm{limit}}$ at t_2, suggest that it is possible to relax the correction action, to reduce EFCCs power supply energy consumption.

The calculation of the EFCCs currents was repeated by solving (10) as a function of the weighting parameter α in its [0,1] range. The normalization coefficients used are: λ_1=30.5 and λ_2=3.64 MJ. The Pareto-front, for the interval Δt_2=3.5 s, is reported in Fig. 3, where w_R is the ohmic contribution.

Due to the specific limitation of *TMEI* in DTT, just the part corresponding to $TMEI_2 \leq 50$ ppm can be actually used (α ∈ [0, 0.47]).

The limit α=0 provides the optimization of just the *TMEI*; in this case, according to the results discussed in the previous section, the *TMEI* approaches very small values (few ppm) but at cost of a high energy demand (more than 8 MJ). If a desired (and prudential) $TMEI_2$ = 40 ppm (80 % of the $TMEI_{\mathrm{limit}}$) is selected from the curve in Fig. 3, corresponding to α=0.42, an energy requirement w_2 of 4.67 MJ is reached, that further decreases to 3.9 MJ at $TMEI_2$ = 50 ppm. Further reduction of the energy demand might be reached, with values in the order of 2 MJ but, unfortunately, at cost of $TMEI_2$ beyond the permitted level.

However, the graph in Fig. 3 is a valuable tool not only in designing phases, but also for the operations, since it provides comprehensive indications for choosing the best compromise between *TMEI* safety margin and energy saving. In Fig. 4, the comparison between the optimized EFCC currents with α=0 and α=0.42 case is shown.

It is worth observing that, due to the resistances and the current values, the ohmic contribution w_R is largely predominant (about two orders of magnitude higher) compared to the other terms (w_L, w_{eq}, and w_{pl}) which represent inductive, equilibrium currents, and plasma contributions respectively (see Table 2).

Similar considerations can be carried out for the subsequent interval

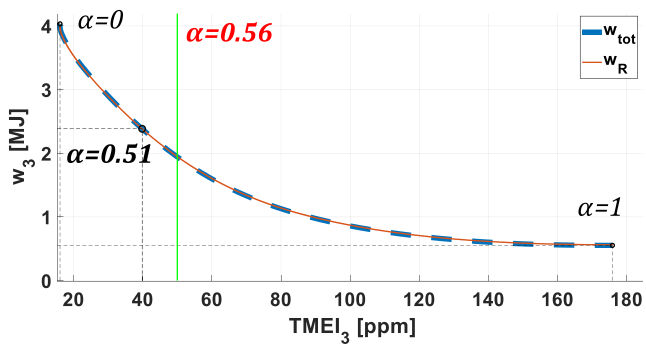

Fig. 5. EFCC energy demand in [t_2, t_3] versus $TMEI_3$ as solution of (10) varying α in [0,1] (blue dashed Pareto front), and its ohmic contribution versus $TMEI_3$ (red Pareto front).

Table 3
Energy contributions in [t_2, t_3] at main α values.

	w_R	w_L	w_{eq}	w_{pl}
α=0	4 MJ	22.7 kJ	0.03 kJ	-4.45 kJ
α=0.51	2.40 MJ	1.71 kJ	-0.17 kJ	-1.42 kJ
α=1	5.62 MJ	-9 kJ	-0.02 kJ	-0.54 kJ

Δt_3=2.75 s. The normalization coefficients used for the second optimization are: λ_1=38.6 and λ_2=3.88 MJ. The Pareto front is shown in Fig. 5 and the comparison between energy consumption contribution at main α values is reported in Table 3.

In this case, α must be limited in the range [0, 0.56] to meet the constraint $TMEI<50$ ppm. The energy demand w_3 for α=0 of about 4 MJ decreases to 2.40 MJ at $TMEI_3$=40 ppm (α=0.51) and further decreases to 1.95 MJ for $TMEI_3$=50 ppm (α=0.56). Further reduction in energy demand (up to about 0.5 MJ for α = 1) could be reached only at cost of prohibited *TMEI* values.

The energy saving for both the intervals corresponds to 40–45 % that would be multiplied for the time intervals for the tokamak lifecycle. A reduction of about 30 % in peak power is also observed, even if this was not the direct target of the optimization. Thus, the tool yields a significant reduction for the power ratings of power supplies and of the electrical systems.

Note that both $TMEI_2$ (in Fig. 3) and $TMEI_3$ (in Fig. 4) obtained for α=1 case, are greater than the initial worst-case *TMEIs*, about 114 ppm and 128 ppm, respectively (see Table 1). In other words, the EFCC currents resulting solely from the energy consumption optimization worsen the *TMEI*, as no EF correction strategy has been applied in these cases. On the contrary, starting from the α=0 case, a halving of power supply energy demand has been observed along with *TMEI* values slightly lower than the permitted threshold.

4. Conclusions

Thanks to the high number of coils independently driven, the EFCC system in DTT exhibits several degrees of freedom. Despite the required high performance and current/voltage constraints, the freedom margins allow for the optimization of the current waveforms with several objectives during a plasma scenario.

If electric energy is considered in the optimization process, significant saving can be achieved. The procedure here proposed provides, for each scenario, a powerful tool for the selection of the EFCC currents during the machine operations, as the best compromise between *TMEI* safety margin and energy saving.

Even though the presented results are focused on the specific EFCC system of DTT, the optimization procedure can be applied and extended for the design and operations of other tokamaks and other types of systems.

CRediT authorship contribution statement

Pasquale Zumbolo: Writing – original draft, Writing – review & editing, Validation, Software, Resources, Methodology, Data curation, Conceptualization, Supervision. **Raffaele Albanese:** Writing – review & editing, Supervision, Conceptualization. **Andrea G. Chiariello:** Writing – review & editing, Supervision, Conceptualization. **Antonio Iaiunese:** Writing – original draft, Writing – review & editing, Validation, Software, Resources, Methodology, Data curation, Conceptualization, Supervision. **Alessandro Lampasi:** Writing – review & editing, Supervision, Data curation, Conceptualization. **Marco Neri:** Writing – review & editing, Supervision. **Raffaele Martone:** Writing – review & editing, Supervision, Conceptualization.

Declaration of competing interest

The authors declare that they have no known competing financial interests or personal relationships that could have appeared to influence the work reported in this paper.

Acknowledgments

The research leading to these results has partially been funded by the PRIN Project P2022KNM7B “TRAINER - Tokamak plasmas daTa-dRiven identificAtIon and magNEtic contRol”, CUP E53D23014670001 funded by EU in NextGenerationEU plan through the Italian “Bando Prin 2022 - D.D. 1409 del 14-09-2022” by MUR. This work was also supported by the Italian Research Ministry under the PRIN Project 2022JCZJ33”. Advanced control techniques for the alternative divertor plasma configurations in nuclear fusion tokamaks”, CUP: E53D23000670006.

Data availability

Data will be made available on request.

References

[1] J. Wesson, D.J. Campbell, *, Tokamaks, 149, Oxford University Press, 2011. *.
[2] R. Sweeney, et al., J. Plasma Phys. 86 (2020) 865860507, https://doi.org/10.1017/S0022377820001129.
[3] R.J. La Haye, R. Fitzpatrick, T.C. Hender, A.W. Morris, J.T. Scoville, T.N. Todd, Critical error fields for locked mode instability in tokamaks, *, Phys. Fluids B: Plasma Phys. 4 (7) (1992) 2098–2103. *.
[4] V.D. Pustovitov, Flux coordinates for tokamaks, *, Plasma Phys. Rep. 24 (6) (1998) 510–520. *.
[5] J.K. Park, A.H. Boozer, J.E. Menard, M.J. Schaffer, Error field correction in ITER, *, Nucl. Fus. 48 (4) (2008) 045006. *.
[6] F. Maviglia, L. Pigatto, F. Villone, H. Zohm, C. Albert, P. Bruzzone, S. Wiesen, Studies on EU-DEMO 3D coils requirements and conceptual design for error field correction and plasma control, Fus. Eng. Des. 196 (2023) 114010.
[7] G. Matsunaga, M. Takechi, S. Sakurai, Y. Suzuki, S. Ide, H. Urano, In-vessel coils for magnetic error field correction in JT-60SA, *, Fus. Eng. Des. 98 (2015) 1113–1117. *.
[8] R. Albanese, T. Bolzonella, A.G. Chiariello, A. Cucchiaro, A. Iaiunese, A. Lampasi, P. Zumbolo, Error field and correction coils in DTT: a preliminary analysis, *, Fus. Eng. Des. 189 (2023) 113437. *.
[9] Martone, R., et al. (2019). *DTT divertor tokamak test facility interim design report*, ENEA ("Green Book"). ISBN 978-88-8286-378-4, https://www.dtt-dms.enea.it/share/s/avvglhVQT2aSkSgV9vuEtw.
[10] V. Amoskov, A. Belov, V. Belyakov, O. Filatov, Y. Gribov, E. Lamzin, S. Sytchevsky, Statistical analysis of expected error fields in tokamaks and their correction, *, Plasma Dev. Oper. 13 (2) (2005) 87–103. *.
[11] M.S. Chu, L.L. Lao, M.J. Schaffer, T.E. Evans, E.J. Strait, Y.Q. Liu, Y. Gribov, Response of a resistive and rotating tokamak to external magnetic perturbations below the Alfvén frequency, Nucl. Fus. 51 (7) (2011) 073036.
[12] H. Reimerdes, A.M. Garofalo, E.J. Strait, R.J. Buttery, M.S. Chu, Y. In, W. M. Solomon, Effect of resonant and non-resonant magnetic braking on error field tolerance in high beta plasmas, Nucl. Fus. 49 (11) (2009) 115001.
[13] A.D. Turnbull, N.M. Ferraro, V.A. Izzo, E.A. Lazarus, J.K. Park, W.A. Cooper, F. Turco, Comparisons of linear and nonlinear plasma response models for non-axisymmetric perturbations, Phys. Plasm. 20 (5) (2013).

[14] P.E. Gill, W. Murray, M.H. Wright, Practical Optimization, *, Academic Press, London, UK, 1981. *.

[15] MathWorks. (2020). Fmincon. Available online: https://www.mathworks.com/help/optim/ug/fmincon.html#busp5fq-6 (accessed on 1 September 2021).

[16] E. van den Berg, M.P. Friedlander, Probing the Pareto frontier for basis pursuit solutions, SIAM J. Sci. Comput. 31 (2) (2009) 890–912, https://doi.org/10.1137/080714488.

[17] K. Miettinen, Nonlinear Multiobjective Optimization, 12, Springer Science & Business Media, 1999.

[18] F. Giorgetti, R. Lombroni, V.G. Belardi, G. Calabrò, M. Dalla Palma, P. Fanelli, F. Vivio, Vertical displacement events analysis using MAXFEA code in combination with ANSYS APDL in the final design stage of the DTT vacuum vessel, Fus. Eng. Des. 184 (2022) 113273.

[19] A. Castaldo, R. Albanese, R. Ambrosino, F. Crisanti, Plasma scenarios for the DTT Tokamak with optimized poloidal field coil current waveforms, Energies 15 (5) (2022) 1702, https://doi.org/10.3390/en15051702.

[20] P. Zumbolo, R. Albanese, A.G. Chiariello, A. Iaiunese, R. Martone, Optimal magnet assembly for error field reduction, IEEE Trans. Plasma Sci. (2024).